Highly Stable Porous Silicon–Carbon Composites as Label-Free Optical Biosensors

Chun Kwan Tsang,[‡] Timothy L. Kelly,[†] Michael J. Sailor,[†,*] and Yang Yang Li[‡,*]

[†]Department of Chemistry and Biochemistry, University of California, San Diego, 9500 Gilman Drive, La Jolla, California 92093-0358, United States and [‡]Department of Physics and Materials Science, City University of Hong Kong, 83 Tat Chee Avenue, Kowloon Tong, Hong Kong, People's Republic of China

ABSTRACT A stable, label-free optical biosensor based on a porous silicon–carbon (pSi–C) composite is demonstrated. The material is prepared by electrochemical anodization of crystalline Si in an HF-containing electrolyte to generate a porous Si template, followed by infiltration of poly(furfuryl) alcohol (PFA) and subsequent carbonization to generate the pSi–C composite as an optically smooth thin film. The pSi–C sensor is significantly more stable toward aqueous buffer solutions (pH 7.4 or 12) compared to thermally oxidized (in air, 800 °C), hydrosilylated (with undecylenic acid), or hydrocarbonized (with acetylene, 700 °C) porous Si samples prepared and tested under similar conditions. Aqueous stability of the pSi–C sensor is comparable to related optical biosensors based on porous TiO_2 or porous Al_2O_3. Label-free optical interferometric biosensing with the pSi–C composite is demonstrated by detection of rabbit IgG on a protein-A-modified chip and confirmed with control experiments using chicken IgG (which shows no affinity for protein A). The pSi–C sensor binds significantly more of the protein A capture probe than porous TiO_2 or porous Al_2O_3, and the sensitivity of the protein-A-modified pSi–C sensor to rabbit IgG is found to be ~2× greater than label-free optical biosensors constructed from these other two materials.

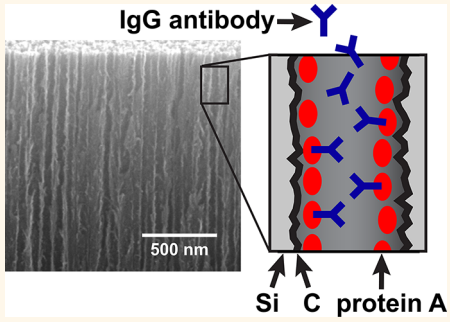

KEYWORDS: mesoporous silicon · carbon · composite · label-free biosensor · optical thin film · Fabry–Perot interference

Porous Si is a promising platform for applications in drug delivery,[1–3] diagnostics,[4–7] and biological sensing,[8–13] owing to its high surface area, its readily tunable pore structure (2–500 nm), and the ease with which it can be formed into complex optical nanostructures such as Bragg stacks,[14,15] rugate filters,[16] and microcavities.[17–20] However, the poor aqueous stability of porous Si remains a major challenge in its medical and biological applications.[21] The operational principle behind porous Si-based interferometric biosensors is a change in refractive index that occurs when aqueous analytes such as proteins or oligonucleotides enter the pores.[22–25] Typically, porous Si-based biosensors contain modified silicon oxide surfaces (SiO_2). Though the Si–O bond is relatively inert in aqueous media, in a nanostructured form, the material slowly hydrolyzes and dissolves in H_2O, causing zero-point drift in the optical biosensor that limits its utility.[21,26,27] More significant dissolution is observed in alkaline media. Many chemical modifications of porous Si have been reported to improve its stability such as hydrosilylation,[28] electrochemical alkylation,[27] and thermal hydrocarbonization.[29] Alternatively, other more stable porous materials have been demonstrated as viable optical interferometric biosensors, such as porous titania (TiO_2)[30,31] and porous alumina (Al_2O_3),[32] although these systems show less flexibility in the design of optical nanostructures or the control of pore size. Recently, a method for placing a stable, mesoporous carbon coating on porous Si was described, involving the extensive pyrolysis of poly(furfuryl alcohol), polymerized *in situ* in a porous Si template.[33] In that work, the carbon coating was found to improve the sensitivity of the resulting material for chemical vapor sensing.[33] In the present work, we use this poly(furfuryl alcohol) chemistry to prepare a porous

* Address correspondence to msailor@ucsd.edu, yangli@cityu.edu.hk.

Received for review June 27, 2012 and accepted November 1, 2012.

Published online November 01, 2012
10.1021/nn304131d

© 2012 American Chemical Society

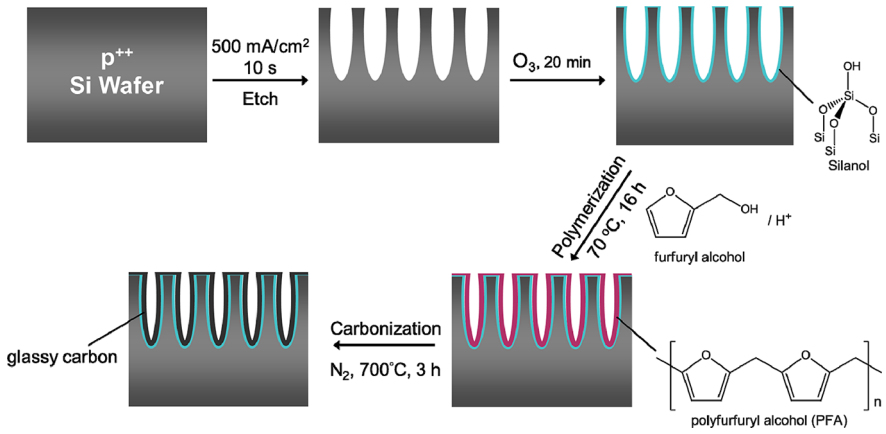

Scheme 1. Synthetic procedure for preparation of the porous Si−C composites used in this study.

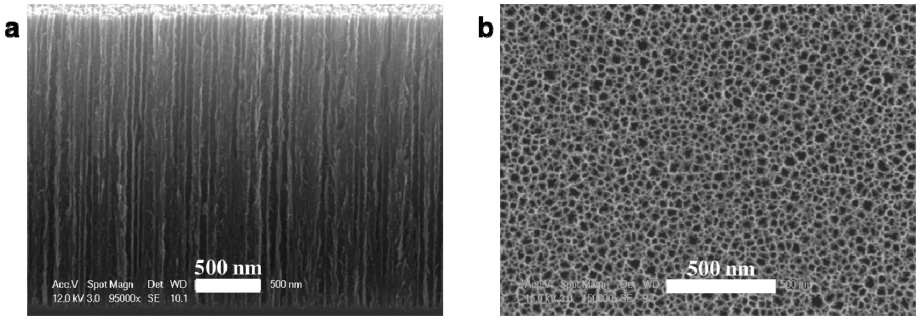

Figure 1. Representative field emission scanning electron microscopy (FESEM) images of the pSi−C composite films used in this study: (a) cross-sectional image, (b) plan-view image. The samples are 2 μm thick, and the pore diameters range from 14 to 42 nm, with an average diameter of 37 nm. Images of the original pSi template and PFA-infiltrated pSi are provided in Figures S3 and S4 in the Supporting Information.

silicon−carbon (pSi−C) composite and find that the material shows excellent stability in aqueous media, enabling a highly stable biosensing platform.

RESULTS AND DISCUSSION

Sample Preparation. The porous silicon−carbon (pSi−C) composites were prepared from porous Si films, following a published procedure,[33] outlined in Scheme 1. A porous Si (pSi) host was first prepared by electrochemical anodization of a highly doped, p-type (p^{++}) single-crystal silicon (100) wafer in an electrolyte consisting of a 3:1 (v/v) solution of aqueous 48% HF and ethanol. The inner pore walls of the resulting pSi film were exposed to ozone to generate a silanol surface. The pores were then infiltrated with a solution of oxalic acid in furfuryl alcohol and heated at 70 °C to polymerize the monomer. The sample was then pyrolyzed in flowing nitrogen to generate the carbon-infiltrated porous silicon (pSi−C) composite. Attenuated total reflectance Fourier transform infrared (ATR-FTIR) spectra of pSi−C at different synthetic stages are shown in Figure S1 in the Supporting Information. Freshly etched pSi (a) shows a Si−H stretching band at 2100 cm^{-1} and a Si−H bending mode at 906 cm^{-1}.[27] After ozone oxidation (b), a broad band centered at 3300 cm^{-1} appears due to O−H stretching of surface silanol groups, together with a band at 1030 cm^{-1}, which is assigned to an asymmetrical Si−O−Si stretching mode.[26] The PFA-infiltrated pSi (c) displays the characteristic bands for PFA at 1560 and 1506 cm^{-1} due to furan ring vibrations and at 2916 cm^{-1} for aliphatic $-CH_2$ stretching.[34] Disappearance of these bands after thermal carbonization of PFA-infiltrated pSi to generate pSi−C composite (d) suggests that the PFA in the pSi was pyrolyzed to glassy carbon. Raman spectroscopy was used to further characterize the carbonaceous material in the pSi−C composite (Figure S2 in the Supporting Information). Two Raman bands were observed at 1330 and 1600 cm^{-1}, which are assigned to D and G bands, respectively. The D band arises from disordered six-membered rings, while the G band is attributed to bond stretching vibrations associated with sp^2-hybridized carbon. The greater intensity of the D band relative to the G band (I_D/I_G = 2.84) suggests the presence of highly disordered sp^2-rich carbon in the pSi−C composite.[35]

Field emission scanning electron microscope (FESEM) measurement reveals no significant change between freshly etched pSi (Figure S3), PFA-infiltrated pSi (Figure S4), and a pSi−C composite (Figure 1), although significant differences were observed in their FTIR spectra. The lack of morphological change detectable by the SEM study suggests that PFA generated in

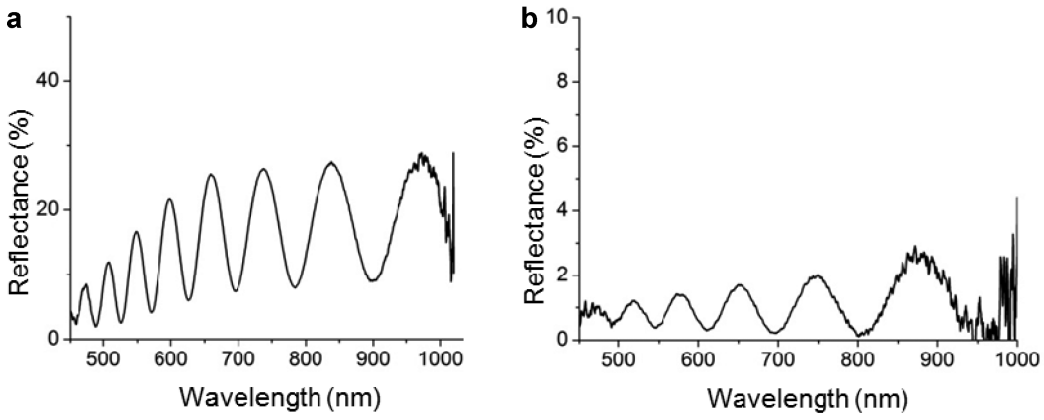

Figure 2. Reflectance spectra (normalized to a mirror with reflectance ≥96%) of (a) the empty pSi template and (b) the pSi−C composite.

the polymerization step forms a very thin coating on the pore walls of pSi, leaving the pores open and unclogged. Plan-view and cross-sectional FESEM images (Figure 1) reveal that the pSi−C composite preserves the high porosity and nanostructure of the precursor porous Si host. The samples contain long, straight pores of ~2 μm length and average diameter of 37 nm. This pore diameter is determined primarily by the etching current density used to prepare the samples (500 mA/cm^2), and it is sufficiently large to accommodate the immunoglobulin analyte (11−17 nm)[36] and protein A capture probe used in the biosensor experiments discussed below.

The pSi−C composite films were sufficiently flat and transparent to display well-resolved Fabry−Pérot interference fringes in the reflectance spectrum. As shown in Figure 2, introduction of carbon reduced the average reflectance of the pSi−C composite significantly compared to the original pSi template (1 and 15%, respectively). The decrease of spectral intensity is attributed to absorption of light by carbon in the pSi−C composite, and the amount of light absorbed by the films was related to the thickness of the pSi−C film. The optical biosensor experiments require distinct Fabry−Pérot interference fringes, which are not discernible in films much thinner than ~1 μm (due to a lack of optical path length) or much thicker than 5 μm (due to optical absorption by carbon). For the optical biosensor measurements, a thickness of ~2 μm was determined to be optimal to minimize absorption while still providing distinct Fabry−Pérot interference fringes.

Analysis of Optical Spectra. The reflectance spectra contain Fabry−Pérot fringes caused by interference of light reflected from the top and bottom interfaces of the porous thin film. The wavelength of the maxima of each of the interference fringes is given by Fabry−Pérot relationship:

$$m\lambda_{max} = 2nL \quad (1)$$

where m is an integer corresponding to the spectral order of the fringe, λ_{max} is the wavelength maximum of the fringe, n is the average refractive index of the porous matrix (including the contents of the pores), and L is the physical thickness of the porous layer. The quantity nL, often referred to as the optical thickness of the film, can be determined directly from the Fourier transform of the reflectance spectrum. The method, called reflective interferometric Fourier transform spectroscopy (RIFTS),[37] provides a convenient means to monitor changes in the optical thickness nL during an optical biosensing experiment. The average refractive index (n) of the porous film generally increases when a protein analyte enters the pores, due to the larger index of proteins relative to water. By contrast, oxidative degradation or dissolution of the porous matrix generally results in a decrease in the value of n.[37]

The porosity and thickness of the pSi−C composite films were determined by optical means, using the spectroscopic liquid infiltration method (SLIM).[38] SLIM is a nondestructive method that fits the change in nL observed when the air in a porous optical film is infiltrated by a liquid of known refractive index. Figure 3a shows the fast Fourier transform (FFT) of a sample in air and after infiltration of ethanol (n = 1.3611). When using ethanol as the liquid infiltrate, fitting of the data using the Bruggeman effective medium approximation[39] yielded values of porosity of 70 ± 1% and a thickness of 2 μm for the pSi−C composites, in agreement with SEM measurements. FFT data resulting from infiltration of an aqueous phosphate buffer solution (PBS, pH 7.4, n = 1.3365), shown in Figure 3b, yielded values for porosity and thickness of 70 ± 1% and 2 μm, respectively. The similarity of the two results (for ethanol and for aqueous buffer) indicate that the pSi−C material is sufficiently hydrophilic, as confirmed by the contact angle measurement results. The contact angle measurements on the pSi−C composite and freshly etched pSi revealed that both samples show reasonable hydrophilicity (contact angle = 58.2 ± 1.2° for the pSi−C composite and 40.2 ± 1.7° for freshly etched pSi; both contact angles <90°) (Figure S5 in the Supporting Information).

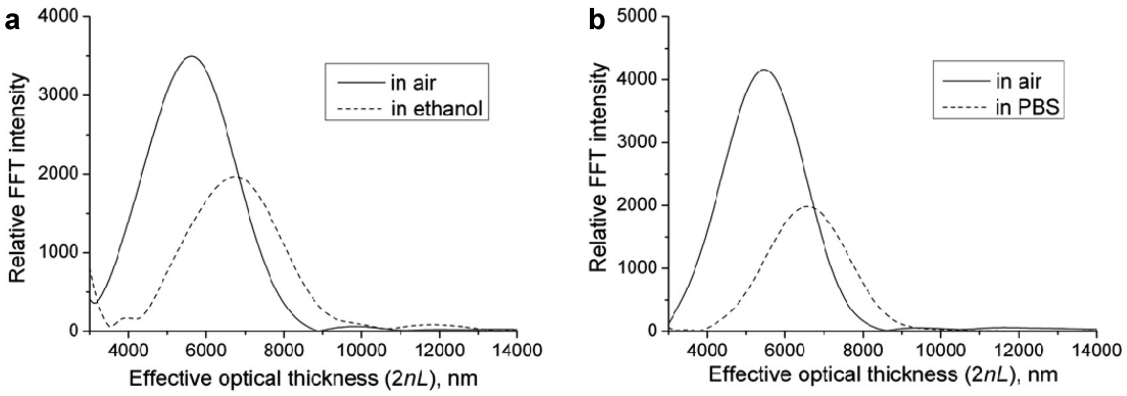

Figure 3. Reflective interferometric Fourier transform spectroscopy (RIFTS) traces for a pSi−C composite sample (a) in air and immersed in ethanol, and (b) in air and immersed in aqueous PBS buffer.

Contact Angle Measurements. The wettability of the pSi−C samples at different stages of the synthesis were evaluated by contact angle measurements (Figure S5, Supporting Information). The water contact angle of freshly etched pSi was measured to be 40.2 ± 1.7° (Figure S5a). Ozone oxidation generates hydrophilic Si−OH species on the surface of pSi, dramatically lowering the contact angle to 5.7 ± 0.3° (Figure S5b). The carbonization treatment increases the contact angle to 58.2 ± 1.2° for the pSi−C composite film, due to the formation of a porous carbonaceous material similar to glassy carbon inside the pores. However, it should be pointed out that the surface of the pSi−C composite was sufficiently wettable to allow infiltration of the protein analytes, as discussed below.

Aqueous Stability Tests. In order to examine the chemical stability of the pSi−C composite film in biologically relevant media, samples were exposed to aqueous buffers and the optical spectra were monitored in real time (Figure 4). The degree of surface degradation can be monitored by the decrease in optical thickness (*nL*) as the porous matrix dissolves. We compared the stability of the pSi−C composite chemistry with three chemical modifications commonly used to stabilize pSi films: acetylene hydrocarbonized pSi,[40] thermally oxidized pSi, and pSi modified by hydrosilylation with undecylenic acid (Scheme 2). The aqueous stability of these surface chemistries in a flowing PBS solution were described in previous work.[41] Figure 4 shows the relative percentage change in optical thickness as a function of time exposed to buffer solutions of pH 7.4 or 12. Here the relative percentage change in optical thickness is defined as

$$\Delta nL/nL_0\% = (nL - nL_0)/nL_0 \times 100\% \qquad (2)$$

where nL_0 is the value of nL (eq 1) measured immediately after introduction of the buffer solution. The decrease in optical thickness observed is indicative of the degradation and subsequent dissolution of the pSi surface. The pSi−C composite shows no significant decrease in optical thickness at pH 7.4 for a period of time of ~75 min. By contrast, the other surface chemistries tested under these conditions display measurable degradation.

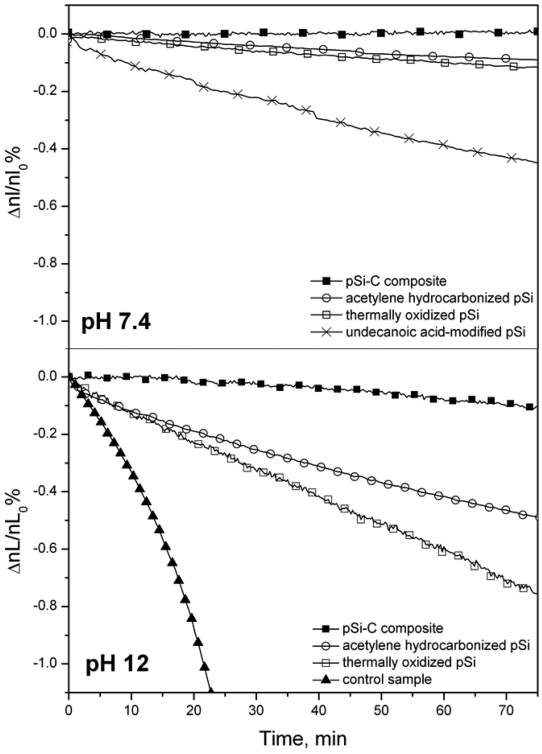

Figure 4. Aqueous stability tests comparing porous Si modification chemistries. Stability monitored optically by reflective interferometric Fourier transform spectroscopy (RIFTS). Top: Samples exposed to flowing (0.5 mL/min) aqueous PBS buffer (pH 7.4). The chemical modifications are as indicated: pSi−C composite (solid squares) is the sample chemistry developed in this work; acetylene hydrocarbonized pSi (open circles), fully oxidized pSi (open squares), and pSi modified by hydrosilylation of undecylenic acid (×) were prepared following the relevant literature procedures (see text). Bottom: Samples exposed to flowing (0.5 mL/min) alkaline buffer (pH 12). Chemical modifications are as indicated in the top plot, with the addition of a control sample consisting of pSi that had been thermally treated similarly to the pSi−C composite but without infiltration of furfuryl alcohol (solid triangles). The relative change in optical thickness, or $\Delta nL/nL_0$% (as defined in eq 2), is plotted against time.

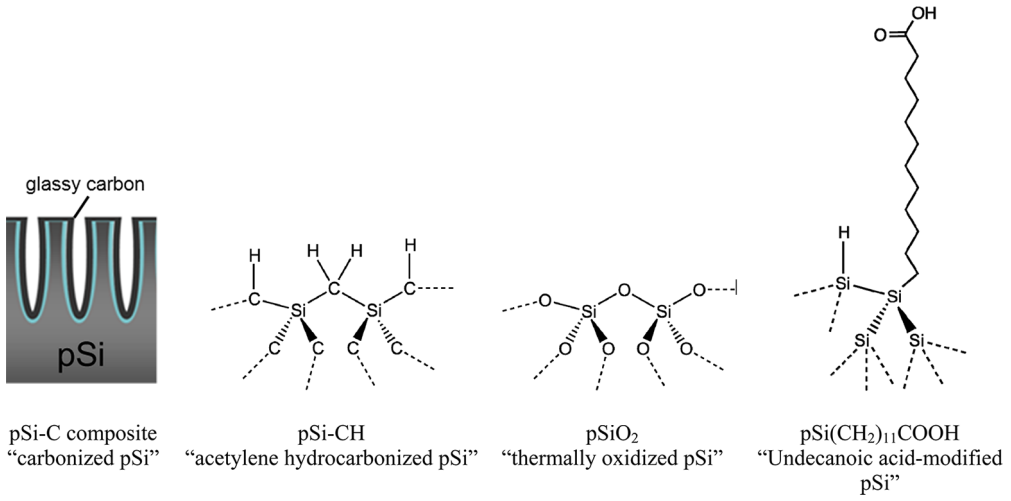

Scheme 2. Depiction of the surface chemistries of porous Si studied in this work. The pSi−C sample was prepared by pyrolysis of poly(furfuryl alcohol) at 700 °C; acetylene hydrocarbonized pSi−CH was prepared by exposure of porous Si to acetylene gas at 700 °C. The thermally oxidized sample was prepared by air oxidation at 800 °C. Undecanoic-acid-modified pSi was prepared by hydrosilylation of undecylenic acid.

The composite film is less stable in highly alkaline media, although it shows significantly greater stability in this solution relative to the other chemistries tested. Hydroxide ion (OH^-) readily attacks both silicon and silica surfaces.[37] When compared to porous silica and acetylene hydrocarbonized pSi, the pSi−C composite exhibits the smallest change in optical thickness, indicating the lowest rate of degradation and dissolution in flowing pH 12 buffer. Consistent with the previous report, acetylene hydrocarbonized pSi shows a smaller degree of degradation (smaller decrease in optical thickness, *nL*) than does porous silica[34] (prepared by complete thermal oxidation of pSi).[41] A control sample, prepared under the same conditions as the pSi−C composite film but without infiltration of the furfuryl alcohol polymer precursor, shows much lower stability at pH 12 than the carbon-passivated sample (Figure 4). From these results, it can be concluded that the carbon produced by carbonization of poly(furfuryl alcohol) provides a strongly passivating layer that prevents oxidative degradation/hydrolysis of the surface.

Immunosensor Experiments. The ability of the pSi−C composite sample to act as a label-free optical biosensor was probed using a protein A capture probe and immunoglobulin G (IgG) analyte. Protein A is a ~42 kDa protein derived from *Staphylococcus aureus* bacteria that binds the F_c domain of the antibody immunoglobulin G (IgG, ~150 kDa), and the protein A/IgG system has several features that make it an attractive benchmark for evaluation of label-free biosensors. First, the affinity of protein A for IgG is species-specific.[42] For example, it binds strongly to rabbit IgG but very weakly to chicken IgG.[43] Thus, chicken IgG can be used as a negative control to test for nonspecific binding of proteins to the sensor surface. In addition, since protein A binds immunoglobulins *via* the F_c domain, the antigen-binding F_{ab} domain is free to bind additional

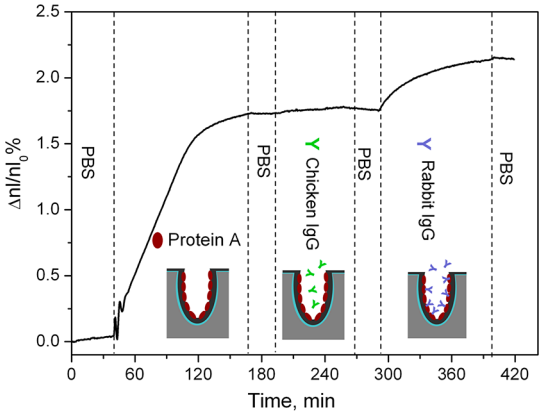

Figure 5. Temporal optical response of the pSi−C biosensor, upon sequential exposure to protein A, chicken IgG, and rabbit IgG. Sample cell was flushed with pure aqueous PBS buffer between analytes, as indicated ("PBS"). The *y*-axis represents the change in optical thickness in %, as defined in eq 2. Flow rate for all solutions was 0.5 mL min^{-1}.

analytes.[32] This allows the evaluation of "cascaded" sensing schemes involving secondary antibodies or sandwich-type assays and the evaluation of the effect of analyte size on biosensor response.[13] The protein A−IgG interaction is also pH-dependent, which allows one to test the reversibility of a sensor system.[13] Finally, protein A has a strong, nonspecific affinity for many inorganic surfaces that avoids the need for covalent attachment chemistries. The adsorbed protein A layer is not readily denatured, retaining at least some of its activity toward binding of IgG, and it tends to minimize nonspecific adsorption of other potentially interfering proteins such as serum albumin.[9]

In this work, the adsorption of rabbit (binding) and chicken (nonbinding) IgG to a protein-A-modified pSi−C surface was monitored by time-resolved measurement of the RIFTS optical response described above. The results of the protein adsorption experiments are

TABLE 1. Comparison of Responses of Optical RIFTS[a] Biosensors to Protein A/IgG Analyte System

material	pore size, nm	porosity	$\Delta nL/nL_0$ %, protein A adsorption	$\Delta nL/nL_0$ %, binding of IgG to preadsorbed protein A	ratio, IgG/protein A binding	ref
porous Al_2O_3	60	40	0.03	0.16	5	32
porous TiO_2	100	40	0.3	0.15	0.5	30
porous SiO_2	40[b]	70% ± 1[b]	1 ± 0.2	0.9 ± 0.1	0.81 ± 0.22	this work
porous Si−C	40	70% ± 1[b]	1.62 ± 0.07	0.41 ± 0.06	0.25 ± 0.02	this work

[a] All sensors compared here operate using the reflective interferometric Fourier transform spectroscopy method. [b] Measured on original pSi film prior to oxidation.

presented in Figure 5 and compared to other porous optical biosensor systems in Table 1. The pSi−C composite film was mounted in an aqueous flow cell that was fitted with an optical window to allow real-time acquisition of spectral reflectance data. Aqueous PBS buffer (pH 7.4) was introduced to the flow cell in order to establish a baseline response. The protein A capture probe (0.1 mg/mL in PBS) was then introduced. The solution was allowed to circulate over the sample for >1 h, and then the cell was flushed with pure buffer solution to remove free or weakly bound protein A. At this point, the change in the measured value of *nL* (relative to the value immediately prior to addition of protein A) was 1.6%. This change is attributed to physical adsorption of protein A in the pSi−C composite film. This percent change (1.6%) is significantly larger than has been observed previously on porous Al_2O_3 (0.03%)[32] or porous TiO_2 (0.3%)[30] optical biosensors and indicates that the pSi−C composite is readily wetted and infiltrated by protein A despite its relatively large contact angle ($58.2 \pm 1.2°$; see above). We prepared a porous SiO_2 sample of similar porosity and pore size as the pSi−C samples (using the same electrochemical etch conditions as for the pSi−C samples) and found the percent change induced by protein A adsorption on porous SiO_2 to be 1%, somewhat smaller than the pSi−C samples (Table 1). The relative binding affinities of all of these surfaces is expected to vary depending on surface area, porosity, and pore size, and so a more quantitative comparison cannot be made here; however, the pSi−C sample appears to display the largest binding affinity for protein A.

Control experiments using chicken IgG were used to determine the specificity of the protein-A-modified surface (Figure 5). Introduction of chicken IgG (0.1 mg/mL) to the protein-A-modified pSi−C sensor resulted in no significant change in optical thickness (quantity *nL*), indicating that chicken IgG did not bind to the protein-A-coated pSi−C composite film, *via* either specific or nonspecific interactions. This result is consistent with the known low affinity of protein A for chicken IgG,[43] as discussed above. The flow cell was then flushed with pure PBS buffer solution, and rabbit IgG was introduced. As shown in Figure 5, the value of *nL* was observed to increase by 0.3% (relative to the baseline measured immediately prior to introduction of rabbit IgG), indicative of a positive binding interaction with the protein A capture probe. In the absence of protein A, IgG binds nonspecifically to the pSi−C surface ($\Delta nL/nL_0 = 0.2\%$, Figure S6, Supporting Information).

While the observed increase in the value of *nL* is consistent with the known ability of rabbit IgG to bind to protein A, the magnitude of the increase is somewhat smaller than would be predicted. As shown in Table 1 and discussed above, although the pSi−C sample adsorbs larger quantities of protein A relative to porous Al_2O_3 or porous TiO_2, the protein-A-modified pSi−C surface appears to be not as efficient at capturing IgG. The optical response of these RIFTS systems scales approximately with analyte mass.[9,13] The mass of IgG is 3.6 times larger than protein A, and so the response to capture of IgG is anticipated to be 3−4 times larger than the response to protein A. Only the porous Al_2O_3 system displays this predicted relationship; the other systems bind significantly less IgG relative to the quantity of protein A adsorbed. The porous Al_2O_3 system also shows the lowest affinity for protein A, and the systems with the highest binding affinity for protein A show the lowest degree of IgG binding. Although the quantity of bound IgG is less, the binding constant for IgG to the protein A surfaces appears to remain large for all of the modified surfaces, as the interaction cannot be reversed simply by rinsing with pure PBS buffer. We propose that the reason for the apparently lower degree of IgG capture is that the IgG binding sites for a large fraction of the protein A molecules are rendered inaccessible due to either denaturing[44] or steric crowding effects[45] of protein A when it undergoes strong binding interactions within the pores. Steric effects on IgG binding have been implicated previously with protein-A-modified porous SiO_2 biosensors; diffusional limits attributed to steric crowding in the pores have been observed in dissociation derivative data.[9] Binding of protein A to porous Al_2O_3, porous TiO_2, and porous SiO_2 is thought to be driven by electrostatic interactions with these negatively charged surfaces,[9,30,32] whereas the more hydrophobic porous Si−C surface may undergo significant van der Waals interactions with protein A that could lead to denaturing and result in the lower degree of IgG capture seen here. It is also possible that the relatively small pore dimensions of the pSi−C sample limits infiltration of IgG. Despite the lower degree of IgG binding to the protein A present on the biosensor surface, the pSi−C film displays a ~2-fold greater

sensitivity to IgG relative to porous Al_2O_3 or porous TiO_2 systems, which is most likely due to the significantly larger quantity of protein A adsorbed on pSi−C.

CONCLUSIONS

When compared to three common chemistries used to stabilize pSi optical biosensors ($pSiO_2$, pSi + alkyl, and pSi + acetylene), the aqueous stability of the pSi−C composite is superior in neutral or highly alkaline aqueous buffer solutions. Compared with porous Al_2O_3 and porous TiO_2 thin film RIFTS configurations that have also been used as label-free optical biosensors for the protein A/IgG system, pSi−C shows comparable (porous TiO_2) or superior (porous Al_2O_3) aqueous stability, and pSi−C shows the greatest physisorption affinity for the protein A capture probe of all sample types considered, though the adsorbed protein A displays significantly reduced activity for subsequent binding of an IgG analyte. The protein-A-coated pSi−C composite sensor is able to capture and detect binding of the rabbit immunoglobulin (IgG) with greater sensitivity than porous Al_2O_3 and porous TiO_2 RIFTS sensors but with lower sensitivity than a porous SiO_2 RIFTS sensor. Similar to these oxide-based sensors that also contain a physisorbed protein A capture probe, the pSi−C sensor shows good selectivity for the target analyte, with no detectable nonspecific binding of a noncompetent (chicken) IgG analyte. Considering its excellent aqueous stability, the pSi−C composite sensor offers the best compromise between aqueous stability and sensitivity for label-free optical biosensing.

EXPERIMENTAL SECTION

Fabrication of Carbon/Porous Silicon Composites. All pSi−C composites in this paper were fabricated using the same procedure. Highly boron-doped, (100)-oriented crystalline silicon wafers with resistivity of 0.9 mΩ·cm were obtained from Siltronix Corp. Electrochemical anodization was carried out in a two-electrode configuration using aqueous HF (48%) in absolute ethanol (3:1 v/v) as the electrolyte. The anodized area of the silicon working electrode was 1.2 cm^2, and a platinum counter electrode was used. To prepare the porous layers, first a sacrificial layer of pSi was fabricated by application of a constant current density of 62.5 mA cm^{-2} for 30 s. The sacrificial layer was dissolved by replacing the electrolyte with an aqueous solution of KOH (2 M) for a few minutes, and the clean wafer was then rinsed with deionized water and ethanol. The wafer was then subjected to a second anodization with a constant current density of 500 mA cm^{-2} for 10 s. The sample containing the porous layer was rinsed with ethanol and dried in a stream of nitrogen gas. The freshly etched sample was oxidized under a flow of ozone gas (1.5 scfh, Ozone Solutions, model OZV-8) for 20 min. The oxidized sample was infiltrated with oxalic acid dihydrate (5 mg mL^{-1}, ACS grade, EMD chemicals) in furfuryl alcohol (98%, Aldrich). The excess solution was gently removed with a tissue, and the sample was then placed in a covered glass Petri dish. The furfuryl alcohol-infiltrated pSi sample was then heated at 70 °C for 16 h to polymerize the monomer. The sample was placed in a tube furnace under flowing nitrogen gas (1 slpm) for 45 min prior to carbonization. After this purging period, the temperature of the furnace was ramped to 700 °C at a heating rate of 10 °C min^{-1}. After 3 h, the furnace was allowed to cool to room temperature under a continuous nitrogen gas flow. To fabricate the control sample used in Figure 4, a freshly etched sample was oxidized under ozone (1.5 scfh) for 20 min. The ozone-oxidized sample was placed in a tube furnace under flowing nitrogen gas (1 slpm) for 45 min. After this purging period, the temperature of the furnace was ramped to 700 °C at a heating rate of 10 °C min^{-1}. After 3 h, the furnace was allowed to cool to room temperature under a continuous nitrogen gas flow.

Fabrication of $pSiO_2$, Acetylene Hydrocarbonized pSi, and Undecylenic-Acid-Modified pSi. These materials were fabricated following the literature procedures.[41] For the pSi-based samples used in the pH 12 stability tests, wafer surfaces were first cleaned by etching a sacrificial layer as described above (anodized at 62.5 mA cm^{-2} for 30 s and then dissolved in 2 M potassium hydroxide). The pSi layer was then prepared by application of a current density of 500 mA cm^{-2} for 10 s. To prepare acetylene hydrocarbonized porous silicon, the above pSi material was placed in a tube furnace and purged with 1 L min^{-1} of N_2 for 15 min prior to introduction of acetylene, then the tube was purged with a constant flux of 1 L min^{-1} of acetylene diluted in 1 L min^{-1} of N_2 for 15 min, and the sample was heated at 700 °C for 45 min. The acetylene flow was stopped, and the furnace was allowed to cool to room temperature under a continuous N_2 flow (1 L min^{-1}) before removal of the sample.

To prepare fully oxidized pSi ($pSiO_2$), the freshly etched pSi sample was heated at 800 °C for 1 h in ambient air. To prepare undecylenic-acid-modified pSi, hydrosilylation of freshly etched pSi was carried out in a Schlenk line under vacuum with undecylenic acid at 130 °C for 2 h. Three freeze−pump−thaw cycles were used to degas the undecylenic acid before the reaction. After reaction, the sample was cleaned with ethanol, acetone, and another rinse of ethanol and dried under N_2.

Optical Interference Spectroscopy. Reflectance spectra were obtained using a tungsten halogen lamp (Ocean Optics, LS1) and a CCD spectrometer (Ocean Optics, USB4000). The tungsten lamp was connected through bifurcated fiber-optic cable to an optical lens, which focused the light onto the biosensor sample, as depicted in Figure S7, Supporting Information. The normal incident light was focused on the sample, and the reflected light was collected through the same optical lens and transferred to the CCD spectrometer *via* the second arm of the bifurcated fiber-optic cable. For reflectance measurements, the spectra were referenced to a silver mirror with $R_s \geq 96\%$ (Newport Corporation). Fourier transform processing of the spectra for RIFTS analysis utilized the published procedure.[37] The Fourier transform of the (intensity *vs* frequency) reflectance spectrum results in a peak whose position on the *x*-axis corresponds to the value of $2nL$ (effective optical thickness). Real-time measurements (time resolution <1 s) were performed to monitor the peak position in the Fourier transform spectrum caused by changes in optical thickness in the biosensing and stability experiment.

Characterization of Porous Materials. Pore size and porous film thickness were determined by field emission scanning electron microscopy (Philips FEG SEM XL30). The porosity was determined using the spectroscopic liquid infiltration method (SLIM),[38] and two raw reflectance spectra were measured on the same spot of the sample when it was dry (in air) and upon immersion in ethanol. RIFTS analysis yielded the two values of nL, and from this, the index of refraction of the porous skeleton the film thickness and the porosity were calculated by fitting to a Bruggeman effective medium approximation.[39] Water contact angles were measured at room temperature using the sessile drop method with water droplets (6 μL) placed at five different spots on the sample surface with a Rame-Hart goniometer (model 500) attached to a CCD camera (30 fps) and DROP image advanced software. Attenuated total reflectance Fourier transform infrared (ATR-FTIR) spectra were recorded using a Thermo Scientific Nicolet 6700 FTIR with a Smart iTR diamond ATR

attachment. The ATR-FTIR spectral resolution was 4 cm^{-1}, and 64 interferograms were averaged per spectrum. Raman spectroscopy was performed on a Renishaw 2000 microscope equipped with a HeNe Laser (632.8 nm).

Optical Biosensor Experiments. The porous thin film sample was placed in a flow cell with a flow rate of 0.5 mL/min, and the optical reflectance spectra were monitored through the transparent window of the flow cell as described above. In a typical experiment, aqueous phosphate buffered saline solution (PBS, 1×, pH 7.4, Gibco, Inc.) was introduced and circulated in a closed loop to establish the baseline for 40 min. A solution of protein A (0.1 mg/mL, EMD calbiochem) in PBS buffer was then introduced to the flow cell and allowed to circulate in a closed loop for 2 h. The flow cell was then flushed with pure PBS buffer solution (open loop) for 30 min to remove any unbound proteins. A solution of chicken IgG (0.1 mg/mL, Jackson ImmunoResearch) in PBS buffer was introduced and circulated in a closed loop through the cell for ~1 h. The sample in the flow cell was then flushed with PBS buffer solution (open loop) for 30 min to remove any free chicken IgG. A solution of rabbit IgG (0.1 mg/mL, Sigma-Aldrich, >95%) in PBS buffer was then introduced and allowed to circulate in a closed loop for >1 h, in order to achieve steady-state saturation binding. Finally, the flow cell was flushed with PBS buffer solution (open loop) for 20 min to determine the stability of the protein/IgG complex assembly.

Stability Tests of Porous Materials in pH 7.4 and pH 12 Buffer Solutions. The pSi−C composite (or other porous material sample) was mounted in the flow cell, and the cell was flushed (flow rate 0.5 mL/min) with phosphate buffered saline (PBS, 1×, pH 7.4, Gibco, Inc.) in a closed loop, and the optical reflectance spectra were monitored through the transparent window of the flow cell as described above. For the pH 12 experiments, the sample cell was first flushed with phosphate buffered saline (PBS, 1×, pH 7.4, Gibco, Inc.) for 15 min to establish a baseline. The sample cell was then flushed with the alkaline buffer (VWR, BDH pH 12 buffer), and the pH 12 solution was circulated in a closed loop while the optical reflectance spectra were recorded for 75 min.

Conflict of Interest: The authors declare no competing financial interest.

Acknowledgment. This work was funded by City University of Hong Kong (Projects 9667056 and 7002741) and by the National Science Foundation under Grant No. DMR-0806859.

Supporting Information Available: Attenuated total reflectance Fourier transform infrared (FTIR-ATR) spectra of pSi−C at different synthetic stages; Raman spectrum of the pSi−C composite; field emission scanning electron microscope (FESEM) images of freshly etched porous silicon samples and PFA-infiltrated pSi in this study; contact angle data for pSi−C composite at different synthetic stages; temporal optical response of the pSi−C biosensor upon exposure to rabbit IgG (without prior adsorption of protein A); schematic diagram of the flow cell setup used in biosensing and aqueous stability experiments. This material is available free of charge *via* the Internet at http://pubs.acs.org.

REFERENCES AND NOTES

1. Wu, E. C.; Andrew, J. S.; Cheng, L. Y.; Freeman, W. R.; Pearson, L.; Sailor, M. J. Real-Time Monitoring of Sustained Drug Release Using the Optical Properties of Porous Silicon Photonic Crystal Particles. *Biomaterials* **2011**, *32*, 1957–1966.
2. Anglin, E. J.; Cheng, L. Y.; Freeman, W. R.; Sailor, M. J. Porous Silicon in Drug Delivery Devices and Materials. *Adv. Drug Delivery Rev.* **2008**, *60*, 1266–1277.
3. Gu, L.; Park, J. H.; Duong, K. H.; Ruoslahti, E.; Sailor, M. J. Magnetic Luminescent Porous Silicon Microparticles for Localized Delivery of Molecular Drug Payloads. *Small* **2010**, *6*, 2546–2552.
4. Park, J. H.; von Maltzahn, G.; Zhang, L. L.; Schwartz, M. P.; Ruoslahti, E.; Bhatia, S. N.; Sailor, M. J. Magnetic Iron Oxide Nanoworms for Tumor Targeting and Imaging. *Adv. Mater.* **2008**, *20*, 1630–1635.
5. Park, J. H.; Gu, L.; von Maltzahn, G.; Ruoslahti, E.; Bhatia, S. N.; Sailor, M. J. Biodegradable Luminescent Porous Silicon Nanoparticles for *In Vivo* Applications. *Nat. Mater.* **2009**, *8*, 331–336.
6. Gossuin, Y.; Disch, S.; Quoc, L. V.; Gillis, P.; Hermann, R. P.; Park, J. H.; Sailor, M. J. NMR Relaxation and Magnetic Properties of Superparamagnetic Nanoworms. *Contrast Media Mol. Imaging* **2010**, *5*, 318–322.
7. Cunin, F.; Schmedake, T. A.; Link, J. R.; Li, Y. Y.; Koh, J.; Bhatia, S. N.; Sailor, M. J. Biomolecular Screening with Encoded Porous-Silicon Photonic Crystals. *Nat. Mater.* **2002**, *1*, 39–41.
8. Schwartz, M. P.; Yu, C.; Alvarez, S. D.; Migliori, B.; Godin, D.; Chao, L.; Sailor, M. J. Using an Oxidized Porous Silicon Interferometer for Determination of Relative Protein Binding Affinity through Non-covalent Capture Probe Immobilization. *Phys. Status Solidi A* **2007**, *204*, 1444–1448.
9. Schwartz, M. P.; Alvarez, S. D.; Sailor, M. J. Porous SiO_2 Interferometric Biosensor for Quantitative Determination of Protein Interactions: Binding of Protein A to Immunoglobulins Derived from Different Species. *Anal. Chem.* **2007**, *79*, 327–334.
10. Pacholski, C.; Yu, C.; Miskelly, G. M.; Godin, D.; Sailor, M. J. Reflective Interferometric Fourier Transform Spectroscopy: A Self-Compensating Label-Free Immunosensor Using Double-Layers of Porous SiO_2. *J. Am. Chem. Soc.* **2006**, *128*, 4250–4252.
11. Lin, V. S. Y.; Motesharei, K.; Dancil, K. P. S.; Sailor, M. J.; Ghadiri, M. R. A Porous Silicon-Based Optical Interferometric Biosensor. *Science* **1997**, *278*, 840–843.
12. Janshoff, A.; Dancil, K. P. S.; Steinem, C.; Greiner, D. P.; Lin, V. S. Y.; Gurtner, C.; Motesharei, K.; Sailor, M. J.; Ghadiri, M. R. Macroporous p-Type Silicon Fabry−Perot Layers. Fabrication, Characterization, and Applications in Biosensing. *J. Am. Chem. Soc.* **1998**, *120*, 12108–12116.
13. Dancil, K. P. S.; Greiner, D. P.; Sailor, M. J. A Porous Silicon Optical Biosensor: Detection of Reversible Binding of IgG to a Protein A-Modified Surface. *J. Am. Chem. Soc.* **1999**, *121*, 7925–7930.
14. Snow, P. A.; Squire, E. K.; Russell, P. S. J.; Canham, L. T. Vapor Sensing Using the Optical Properties of Porous Silicon Bragg Mirrors. *J. Appl. Phys.* **1999**, *86*, 1781–1784.
15. Vincent, G. Optical-Properties of Porous Silicon Superlattices. *Appl. Phys. Lett.* **1994**, *64*, 2367–2369.
16. Salem, M. S.; Sailor, M. J.; Sakka, T.; Ogata, Y. H. Electrochemical Preparation of a Rugate Filter in Silicon and Its Deviation from the Ideal Structure. *J. Appl. Phys.* **2007**, *101*, 063503.
17. Salem, M. S.; Sailor, M. J.; Harraz, F. A.; Sakka, T.; Ogata, Y. H. Electrochemical Stabilization of Porous Silicon Multilayers for Sensing Various Chemical Compounds. *J. Appl. Phys.* **2006**, *100*, 083520.
18. Ouyang, H.; DeLouise, L. A.; Miller, B. L.; Fauchet, P. M. Label-Free Quantitative Detection of Protein Using Macroporous Silicon Photonic Bandgap Biosensors. *Anal. Chem.* **2007**, *79*, 1502–1506.
19. De Tommasi, E.; Rea, I.; Rendina, I.; Rotiroti, L.; De Stefano, L. Protein Conformational Changes Revealed by Optical Spectroscopic Reflectometry in Porous Silicon Multilayers. *J. Phys.: Condens. Matter* **2009**, *21*, 035115.
20. De Stefano, L.; Rotiroti, L.; De Tommasi, E.; Rea, I.; Rendina, I.; Canciello, M.; Maglio, G.; Palumbo, R. Hybrid Polymer-Porous Silicon Photonic Crystals for Optical Sensing. *J. Appl. Phys.* **2009**, *106*, 023109.
21. Alvarez, S. D.; Derfus, A. M.; Schwartz, M. P.; Bhatia, S. N.; Sailor, M. J. The Compatibility of Hepatocytes with Chemically Modified Porous Silicon with Reference to *In Vitro* Biosensors. *Biomaterials* **2009**, *30*, 26–34.
22. Bonanno, L. M.; Segal, E. Nanostructured Porous Silicon-Polymer-Based Hybrids: From Biosensing to Drug Delivery. *Nanomedicine* **2011**, *6*, 1755–1770.
23. Bonanno, L. M.; Kwong, T. C.; DeLouise, L. A. Label-Free Porous Silicon Immunosensor for Broad Detection of Opiates in a Blind Clinical Study and Results Comparison to Commercial Analytical Chemistry Techniques. *Anal. Chem.* **2010**, *82*, 9711–9718.

24. Weiss, S. M.; Rong, G.; Lawrie, J. L. Current Status and Outlook for Silicon-Based Optical Biosensors. *Physica E* **2009**, *41*, 1071–1075.
25. Jane, A.; Dronov, R.; Hodges, A.; Voelcker, N. H. Porous Silicon Biosensors on the Advance. *Trends. Biotechnol.* **2009**, *27*, 230–239.
26. Gao, T.; Gao, J.; Sailor, M. J. Tuning the Response and Stability of Thin Film Mesoporous Silicon Vapor Sensors by Surface Modification. *Langmuir* **2002**, *18*, 9953–9957.
27. Lees, I. N.; Lin, H. H.; Canaria, C. A.; Gurtner, C.; Sailor, M. J.; Miskelly, G. M. Chemical Stability of Porous Silicon Surfaces Electrochemically Modified with Functional Alkyl Species. *Langmuir* **2003**, *19*, 9812–9817.
28. Webb, L. J.; Lewis, N. S. Comparison of the Electrical Properties and Chemical Stability of Crystalline Silicon-(111) Surfaces Alkylated Using Grignard Reagents or Olefins with Lewis Acid Catalysts. *J. Phys. Chem. B* **2003**, *107*, 5404–5412.
29. Salonen, J.; Bjorkqvist, M.; Laine, E.; Niinisto, L. Stabilization of Porous Silicon Surface by Thermal Decomposition of Acetylene. *Appl. Surf. Sci.* **2004**, *225*, 389–394.
30. Mun, K. S.; Alvarez, S. D.; Choi, W. Y.; Sailor, M. J. A Stable, Label-Free Optical Interferometric Biosensor Based on TiO_2 Nanotube Arrays. *ACS Nano* **2010**, *4*, 2070–2076.
31. Song, Y. Y.; Schmuki, P. Modulated TiO_2 Nanotube Stacks and Their Use in Interference Sensors. *Electrochem. Commun.* **2010**, *12*, 579–582.
32. Alvarez, S. D.; Li, C. P.; Chiang, C. E.; Schuller, I. K.; Sailor, M. J. A Label-Free Porous Alumina Interferometric Immunosensor. *ACS Nano* **2009**, *3*, 3301–3307.
33. Kelly, T. L.; Gao, T.; Sailor, M. J. Carbon and Carbon/Silicon Composites Templated in Rugate Filters for the Adsorption and Detection of Organic Vapors. *Adv. Mater.* **2011**, *23*, 1776–1781.
34. Burket, C. L.; Rajagopalan, R.; Marencic, A. P.; Dronvajjala, K.; Foley, H. C. Genesis of Porosity in Polyfurfuryl Alcohol Derived Nanoporous Carbon. *Carbon* **2006**, *44*, 2957–2963.
35. Yahya, N. *Carbon and Oxide Nanostructures: Synthesis, Characterisation and Applications*; Springer: Heidelberg, 2011; Vol. 5, p 88.
36. Saphire, E. O.; Parren, P. W. H. I.; Barbas, C. F.; Burton, D. R.; Wilson, I. A. Crystallization and Preliminary Structure Determination of an Intact Human Immunoglobulin, b12: An Antibody That Broadly Neutralizes Primary Isolates of HIV-1. *Acta. Crystallogr., D* **2001**, *57*, 168–171.
37. Sailor, M. J. *Porous Silicon in Practice: Preparation, Characterization, and Applications*, 1st ed.; Wiley-VCH: Weinheim, Germany, 2012; p 250.
38. Segal, E.; Perelman, L. A.; Cunin, F.; Di Renzo, F.; Devoisselle, J. M.; Li, Y. Y.; Sailor, M. J. Confinement of Thermoresponsive Hydrogels in Nanostructured Porous Silicon Dioxide Templates. *Adv. Funct. Mater.* **2007**, *17*, 1153–1162.
39. Pacholski, C.; Sartor, M.; Sailor, M. J.; Cunin, F.; Miskelly, G. M. Biosensing Using Porous Silicon Double-Layer Interferometers: Reflective Interferometric Fourier Transform Spectroscopy. *J. Am. Chem. Soc.* **2005**, *127*, 11636–11645.
40. Torres-Costa, V.; Martin-Palma, R. J.; Martinez-Duart, J. M.; Salonen, J.; Lehto, V. P. Effective Passivation of Porous Silicon Optical Devices by Thermal Carbonization. *J. Appl. Phys.* **2008**, *103*, 083124.
41. Sciacca, B.; Alvarez, S. D.; Geobaldo, F.; Sailor, M. J. Bioconjugate Functionalization of Thermally Carbonized Porous Silicon Using a Radical Coupling Reaction. *Dalton Trans.* **2010**, *39*, 10847–10853.
42. Lindmark, R.; Biriell, C.; Sjoquist, J. Quantitation of Specific IgG Antibodies in Rabbits by a Solid-Phase Radioimmunoassay with I-125-Protein-A from *Staphylococcus-aureus*. *Scand. J. Immunol.* **1981**, *14*, 409–420.
43. Harlow, E; Lane, D. *Antibodies—A Laboratory Manual*; Cold Spring Harbor Laboratory Press: Cold Spring Harbor, NY, 1988.
44. Feng, L.; Andrade, J. D. Protein Adsorption on Low-Temperature Isotropic Carbon: I. Protein Conformational Change Probed by Differential Scanning Calorimetry. *J. Biomed. Mater. Res.* **1994**, *28*, 735–743.
45. Bonanno, L. M.; DeLouise, L. A. Steric Crowding Effects on Target Detection in an Affinity Biosensor. *Langmuir* **2007**, *23*, 5817–5823.